ADVANCED ENERGY & SUSTAINABILITY RESEARCH
Open Access
www.advenergysustres.com

Comparative Analysis of Hydrogen Production and Economic Feasibility: Direct versus Indirect Coupling of Photovoltaic Systems with Electrolyzers

Alfonso González del Valle, Pablo García-Linares, and Antonio Martí*

Hydrogen production using photovoltaics (PV) is essential for decarbonizing many sectors of the economy. The integration of PV and hydrogen electrolyzers is actively debated, with focus on direct versus indirect configurations and the option of storage. Direct configuration connects PV directly to the electrolyzer, offering simplicity and reduced installation costs but depends on the weather for efficient power transfer. Indirect configuration adds a power stage, increasing complexity and losses, but enabling maximum power tracking. Adding batteries allows storage of excess PV energy, extending hydrogen production. This study optimizes a PV generator to maximize annual hydrogen production in the direct configuration, then uses the same PV array for indirect configurations with and without batteries for a fair comparison. Results show that the indirect configuration with a battery yields 78% more hydrogen annually than without a battery and 109% more than the direct configuration. The indirect configuration with a battery uses 86.9% of PV energy for hydrogen production, yielding the highest profit at 2.53 $€ \cdot W^{-1}$ (euros per watt-peak of PV), compared to the direct and indirect configurations without a battery, which use 41.9% and 44.6% of PV energy and generate 1.49 and 1.83 $€ \cdot W^{-1}$, respectively.

1. Introduction

The energy transition aims to reduce dependence on fossil fuels, decrease greenhouse gas emissions, promote renewable energies, and enhance energy efficiency. In this context, renewable hydrogen (H_2) has emerged as a key player in the transition[1] because of its potential ability to serve as an alternative in sectors where electrification is not feasible such as steel,[2] cement,[3] and chemical production,[4] which require high temperatures and continuous processes. Maritime and air transport are also challenging for electrification due to long distances and the need for high energy density.[5,6] Beyond heavy industries and transport, H_2 can also play a transformative role in agriculture, particularly in remote rural areas with insufficient electrical infrastructure,[7] and in mining operations in isolated locations with high energy demands.[8,9] Although it is not a difficult-to-electrify application, H_2 is also crucial to produce fertilizers such as ammonia.[10]

Solar-hydrogen (S-H) systems use photovoltaic (PV) electricity to produce H_2. Their main components are the PV generator, which converts sunlight into electric energy, and the electrolyzer, which uses this electric energy to split water into H_2 and oxygen (O_2). S-H systems, where the electrolyzer input is directly connected to the electrical output of the PV generator, are known as direct coupling configurations (**Figure 1**).[11–13] On the contrary, systems with an indirect configuration incorporate an intermediate power stage (PS) to bias the PV generator at its maximum power point (MPP) and transfer this power to the electrolyzer (Figure 1b). In this context, the maximum power point tracker (MPPT) ensures the maximization of PV power generation as meteorological conditions vary, while the DC–DC converter accommodates the output voltage provided by the MPPT to the input voltage of the electrolyzer, maximizing its operational power. The MPP is defined as the product of I_{MPP} and V_{MPP} where they respectively stand for the maximum power point current and output voltage of the PV generator at a particular irradiance and temperature conditions (Figure 1b). Equivalently, the electrolyzer input power is given by the product of I_{EL} and V_{EL}, where these stand for the electrolyzer current and voltage, respectively.[14]

Given the intermittent availability of renewable energy sources (RES), H_2 production in S-H systems can fluctuate. The peak power output (W_p) of a PV generator under standard test conditions (STC), is only reached during specific times of the day. Thus, to ensure that the PV generator can reliably power the electrolyzer, it is necessary to oversize its power relative to the electrolyzer requirements. Proceeding in this way, it is also likely that the PV array will produce for some periods of time more power than the electrolyzer can take, generating an energy surplus not used instantaneously. Storing this surplus energy from the PV generator in batteries helps stabilize H_2

A. González del Valle, P. García-Linares, A. Martí
ETSI Telecomunicación
Instituto de Energía Solar—Universidad Politécnica de Madrid
Ciudad Universitaria, 28040 Madrid, Spain
E-mail: p.garcia-linares@upm.es

The ORCID identification number(s) for the author(s) of this article can be found under https://doi.org/10.1002/aesr.202400210.

© 2024 The Author(s). Advanced Energy and Sustainability Research published by Wiley-VCH GmbH. This is an open access article under the terms of the Creative Commons Attribution License, which permits use, distribution and reproduction in any medium, provided the original work is properly cited.

DOI: 10.1002/aesr.202400210

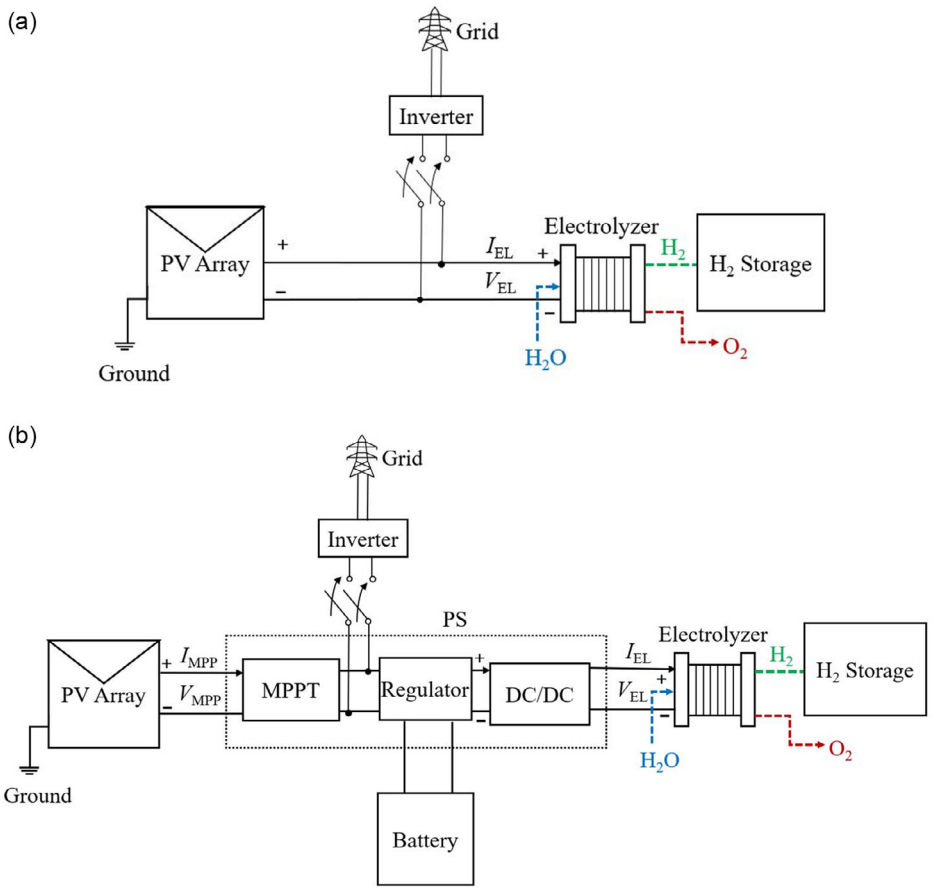

Figure 1. a) Schematic of a solar-hydrogen (S-H) system with a direct configuration, consisting of a PV array, an electrolyzer, H_2 storage, and the grid connection. b) Schematic of S-H systems with different indirect configurations, both include the elements of the indirect configuration and the power stage (PS). One configuration features a regulator and a battery, while the other does not.

production.[15–17] Indirect systems are particularly adaptable for this purpose by only adding a battery and a regulator (as shown in Figure 1), enhancing their versatility. The regulator, as well as the MPPT and DC/DC converter are common elements used in more conventional systems where the energy from the PV generator needs to be coupled to other loads different from electrolyzers. In this regard, lithium-ion batteries offer significant advantages over other battery technologies. Firstly, they have a high energy density, allowing them to store a large amount of energy relative to their size and weight.[16,17] Secondly, lithium-ion batteries typically have a longer lifespan and can endure more charge–discharge cycles compared to alternative battery technologies, making them cost-effective.[18,19]

The advantages and disadvantages of each configuration continue to be a topic of debate. In favor of direct coupling one could argue that, with proper design of the PV array and electrolyzer, this configuration can operate the electrolyzer near its MPP effectively, with coupling factors up to 90%,[11,20–23] making it economically advantageous, as it eliminates the costs associated with electronic coupling systems ($0.045\ €\cdot W^{-1}$).[21,24,25] This work builds on a previously published study by the authors,[26] which compared H_2 production between systems with direct and indirect coupling. The present work goes further by also considering the use of batteries in the indirect system to store excess energy and use it as needed. Given these considerations, this article will compare, both energetically and economically, the annual performance of three PV-to-electrolyzer coupling configurations: direct, indirect, and indirect with a battery for energy storage. For that, the optimal strategy for maximizing H_2 production will be determined with the same annual solar energy input. The comparison will provide detailed insights into energy production, energy usage, and H_2 output. Moreover, an economic feasibility study of the three configurations will be conducted to determine which generates the highest net benefits. The main contribution of this article is that it expands and deepens the comparative analysis of both direct and indirect configurations in terms of overall efficiency and cost-effectiveness. This article also addresses the inclusion of batteries for hydrogen production, which has been studied in direct coupling[27–32] and indirect coupling.[23,33,34] Specifically, it delves into the effects of incorporating batteries on the performance of the indirect configuration. The models used for the incident irradiance, PV generator, PS, battery, and electrolyzer will be discussed first in Section 2.1–2.4.

© 2024 The Author(s). Advanced Energy and Sustainability Research published by Wiley-VCH GmbH

2. System Models

The calculation of the annual H_2 production from the PV generator energy output involves 1) obtaining annual data of irradiance (G_t) and temperature (T) at the site where the PV generator is located, 2) modeling the PV generator output power from the given G_t and T, and 3) modeling the electrolyzer that transforms electric energy and water into H_2 and O_2. In the case of indirect configuration, the PS and the battery (when coupled) are also simulated.

2.1. Irradiance and Temperature Operating Conditions

The initial stage of the simulation involves obtaining G_t and T data for every hour from a typical meteorological year (January 1st to December 31st), totaling 8,760 h, at a specific location. For this study, we have chosen Madrid, Spain, located at coordinates (40.453N, −3.727E), corresponding to the Solar Energy Institute at the Technical University of Madrid, where this research is being conducted. The data were sourced from the PVGIS-SARAH2[35] database on a fixed plane with optimal tilt and azimuth angles of 36° and 0°, respectively. In this location, the total incident energy on the PV generator throughout the year is 2.79 MWh m^{-2}.

2.2. PV Generator Characteristics

The building block of the PV generator is the solar cell. Its current–voltage characteristic will be modeled according to the single diode model (SDM)[36–38]

$$I_c = J_c A_c = I_{ph,c} - I_{0,c}\left(\exp\frac{qV_c + qR_{s,c}I_c}{nk_BT} - 1\right) - \frac{V_c + R_{s,c}I_c}{R_{sh,c}} \quad (1)$$

where I_c is the current through the cell, J_c is the current density, A_c is the area of the cell, $I_{ph,c}$ is the photogenerated current of the solar cell, $I_{0,c}$ is the reverse saturation current of the solar cell, q is the charge of the electron in absolute value, V_c is the output voltage of the solar cell, $R_{s,c}$ is the series resistance of the solar cell, $R_{sh,c}$ is the shunt resistance of the solar cell, k_B is the Boltzmann's constant and n is the diode ideality factor of the solar cell.

In a PV module, N_s solar cells are connected in series to increase the output voltage. To increase further the module current, identical N_p strings of the previous N_s solar cells connected in series can be connected in parallel. When this is done, the current–voltage characteristic of the module (I_{PV}–V_{PV}) is given by:[39,40]

$$I_{PV} = N_p\left[I_{ph,c} - I_{0,c}\left(\exp\frac{qV_{PV}/N_s + qR_{s,c}I_{PV}/N_p}{nk_BT} - 1\right) - \frac{V_{PV} + N_sR_{s,c}I_{PV}/N_p}{N_sR_{sh,c}}\right] \quad (2)$$

The modules can be connected in series with other PV modules to increase the output voltage of the generator, or in parallel to enhance the output current. However, for the sake of simplicity, we will focus on the scenario where the PV generator consists of a single module with all its solar cells connected in series ($N_p = 1$, $N_s \geq 1$). The reason is that this setup allows for optimizing output current and voltage by adjusting the solar cell area while maintaining simplicity and not affecting the results. The parameters of the solar cell that constitute the building block of this module were chosen, initially, so that the PV module exhibits a nominal power of 200 W_p at STC and an efficiency approaching that of silicon commercial modules (20%), which leads to a module area $A = 1\ m^2$. We chose a nominal power of 200 W_p in order to make it easily scalable and to effectively illustrate our points. A_c and N_s parameters were then optimized to maximize annual H_2 production under direct configuration throughout the whole typical meteorological year.[26] The same parameters are used for the rest of configurations studied, since the presence of the PS makes the PV generator to always operate optimally. **Table 1** collects the parameters of the PV cell and the PV module, including the resulting values for the short-circuit current (I_{SC}), open-circuit voltage (V_{OC}), fill factor (FF), I_{MPP}, and V_{MPP} at STC of the PV module.

Figure 2 shows a family of the I_{PV}–V_{PV} characteristics of the PV module as a function of different G_t, from 100 to 1000 W m^{-2}, where the direct relationship between G_t and photogenerated current can be observed. The maximum power (P_{MPP}) of the PV module for each of the different G_t is calculated and indicated within the I_{PV}–V_{PV} curve with round markers.

Table 1. PV cell and module parameters (at STC) used in the simulations.

Cell parameter		Module parameter	
Cell area, A_c [cm^2]	417	Module area, A [m^2]	1
Reverse saturation current density, $J_{0,c}$ [A cm^{-2}][60]	8.14×10^{-12}	Short circuit current, I_{SC} [A]	14.24
Photogenerated current density, $J_{ph,c}$ [mA cm^{-2}][61]	34.1	Open circuit voltage, V_{OC} [V]	17.38
Cell series resistance, $r_{s,c}$ [Ω cm^2][62]	19.9	Current at the maximum power point, I_{MPP} [A]	13.52
Cell shunt resistance, $r_{sh,c}$ [kΩ cm^2][62]	147	Voltage at the maximum power point, V_{MPP} [V]	14.83
Cell diode ideality factor, n[63]	1.18	Fill factor, FF	0.810
Temperature coefficient, α[64]	3.20×10^{-3}	Efficiency, η_m [%]	20.0
Band gap, E_g [eV][65]	1.10	Number of cells in series, N_s	24

© 2024 The Author(s). Advanced Energy and Sustainability Research published by Wiley-VCH GmbH

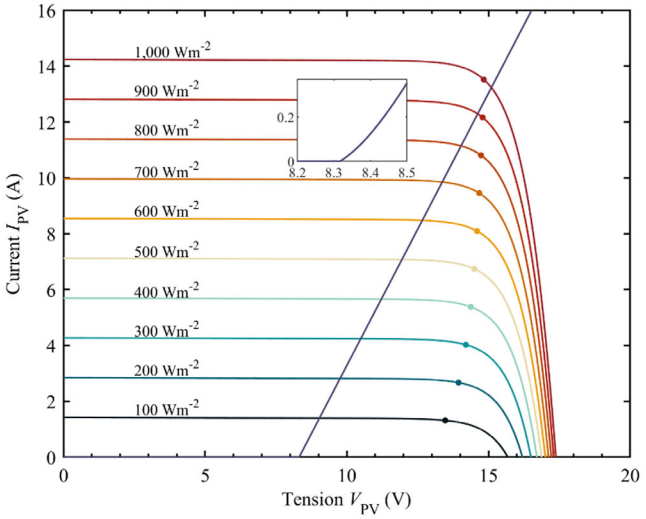

Figure 2. Curren–voltage curves of the 200 W_p optimized PV module (24 cells) for G_t 100–1000 W m^{-2} with corresponding MPP and the electrolyzer. The inset shows the electrolyzer curve at voltage values very close to $V_{th,EL}$.

The logarithmic increase of the module voltage with G_t (and correspondingly, with photogenerated current) makes the V_{OC} and the MPP move to higher values as the irradiance increases.

2.3. Electrolyzer Model

The electrolyzer converts electrical energy into chemical energy by splitting H_2O into H_2 and O_2. For our analysis, we will use proton exchange membrane (PEM) electrolyzers due to their operational flexibility, making them ideal for intermittent application such as renewable energy utilization.[41,42] In this technology, the anode (oxidation electrode) and cathode (reduction electrode) are separated by a solid polymeric PEM. The electrodes and membrane assembly is known as the electrolytic cell, which can be connected in series with other cells, forming the stacking.[43] The chemical reaction that splits H_2O into H_2 and O_2 requires a minimum electrical work to happen. This energy appears in the electrolyzer as the minimum voltage ($V_{rev} = 1.23$ V)[44] at standard conditions of pressure and temperature (1 atm, 298 K). In practice, additional electric work has to be supplied due to the absence of an external heat source that preserves the temperature constant as well as the existence of irreversible processes. Hence, the threshold voltage of a cell ($V_{th,c}$) needed for the mentioned reaction to occur is greater than V_{rev}. Based on our experience with electrolyzers, a reasonable $V_{th,c}$ is 1.38 V.[26] As current flows through the cell, the actual reaction voltage exceeds $V_{th,c}$ due to additional internal losses. These losses are accounted for by overpotentials, so the voltage of the electrolytic cell ($V_{EL,c}$) is given by:

$$V_{EL,c}(I_{EL}) = V_{th,c} + V_{act}(I_{EL}) + V_{con}(I_{EL}) + V_{ohm}(I_{EL}) \quad (3)$$

where V_{act} is the activation overpotential, V_{con} is the concentration overpotential, and V_{ohm} is the ohmic overpotential.[24,43,45,46]

To simulate the electrolyzer we used the same model as in our previous study (see the Appendix).[26] The electrolyzer parameters in both studies are identical, except for the electrolyzer area, which has been increased from 5 to 8.75 cm^2. This change in the electrolyzer area ensures that $V_{th,c}$ remains consistent with the previous study and that the I_{EL}, which depends on the now higher I_{PV} due to the resizing of the PV module, is associated with the same current densities as in the previous study. We selected the cell area of 8.75 cm^2 so that at 65 W, which corresponds to the maximum value of I_{EL}, the current density never exceeds 4 A cm^{-2}. This limit was set to prevent the occurrence of phenomena associated with concentration overpotential (See Table A1 in the Appendix). Similarly to the PV module, the electrolyzer stack used for our study consists of multiple identical electrolytic cells connected in series. These cells share the same current (I_{EL}) and their individual voltages ($V_{EL,c}$) contribute to the total stack voltage ($V_{EL} = V_{EL,c} \cdot S_{cell}$), where S_{cell} denotes the number of cells in series. Since V_{EL} depends on S_{cell} and considering that each electrolytic cell has its own $V_{th,c}$, the V_{th} of the electrolyzer is given by $V_{th} = V_{th,c} S_{cell}$.

Figure 2 depicts a typical current–voltage characteristic of the electrolyzer, where I_{EL} is 0 for $V_{EL} < V_{th}$, but starts increasing once the threshold voltage V_{th} is exceeded. In our model, the electrolyzer contains six cells connected in series, what gives $V_{th} = 8.33$ V, as shown in Figure 2. The electrolyzer used in our simulations has a nominal power of 65 W_p, which is a reasonable ratio between nominal PV power to electrolyzer power for this application. After calculating the current–voltage characteristic of the electrolyzer, the subsequent step involves determining the amount of H_2 ($\dot{m}H_2$) produced via the Faradaic law of electrolysis:

$$\dot{m}H_2 = \frac{I_{EL} S_{cell} \mu_F}{2F} \quad (4)$$

where I_{EL} is the current through the electrolyzer, μ_F is the Faradaic efficiency (99% in PEM),[47] and F is the Faraday constant (96 500 C mol^{-1}). Note that I_{EL} considers the losses associated by overpotentials (activation, concentration, and ohmic) on the electrolyzer, as it is related to V_{EL} through the $I_{EL} - V_{EL}$ characteristic (3). The cumulative H_2 production (MH_2) can be calculated by integrating its production rate throughout the year. Note that in this study, the electrolyzer produces H_2 at up to 65 W. If the power provided to the electrolyzer exceeds this limit, it is considered excess power in our calculations. This maximum operating power limit of the electrolyzer was not established in our previous study.[26]

2.4. Battery Model

Indirect configuration may also incorporate batteries to store surplus energy generated by the PV module. The battery is used to store energy and power the electrolyzer during periods when PV energy is insufficient, thereby extending H_2 production throughout the year. Specifically, a lithium-ion battery is connected between the PS and the PEM electrolyzer through a regulator that prioritizes power transfer to the load, that is, H_2 production, over battery charging. Consequently, the battery only charges if the PV module generates sufficient energy to power the electrolyzer at

© 2024 The Author(s). Advanced Energy and Sustainability Research published by Wiley-VCH GmbH

its nominal operating point (65 W), and the state of charge (SOC) of the battery is below its maximum capacity. The SOC of the battery is defined as:

$$\mathrm{SOC} = \frac{C_{\mathrm{bat}}}{C_{\mathrm{max}}} \tag{5}$$

where C_{bat} is the instantaneous value of the capacity of the battery and C_{max} is the maximum capacity. In this study, the SOC varies between 0.2 and 1 to prevent overcharging and overdischarging of the battery. Moreover, the battery will supply energy whenever the 200 W_p PV module cannot provide enough power to reach the electrolyzer at 65 W_p under the following conditions: 1) during nighttime and 2) during daytime when the module fails to reach 65 W_p. In such cases, the battery supplements the energy to meet the 65 W_p requirement, but if insufficient, it provides whatever energy it can supply. These scenarios assume that the SOC remains above the minimum. If the SOC drops to the minimum level, the battery ceases to supply energy to the electrolyzer. Conversely, if the battery reaches its maximum SOC and the PV module generates enough energy to power the electrolyzer at 65 W, any surplus energy will be fed into the grid. The C_{max} in the indirect configuration has been optimized to ensure maximum profitability of the indirect configuration over the PEM electrolyzer lifespan. This optimization is crucial as the battery represents a significant initial investment, which could make the indirect configuration with the battery economically unviable. The optimal battery C_{max} is the one that maximizes profitability in this setup, considering both the battery cost and the utilization rate of PV energy, which is the ratio of the energy provided by the battery to the electrolyzer and the total PV energy of the indirect configuration. Specifically, batteries with capacities of 1800, 1350, 900, and 450 Wh were selected for simulation testing since these values are close to industry standards and served as an initial assessment range. The results are summarized in **Table 2**, where the CAPEX of the configuration increases with the battery capacity. The PV rate also increases with the battery capacity; however, it stabilizes significantly beyond 900 Wh, with only a marginal difference (1.41%) observed between 900 and 1800 Wh. Table 2 further indicates that the 900 Wh battery provides the highest net profitability for the indirect configuration after 9 years. This outcome is attributed to the fact that, while higher battery capacities lead to increased H_2 production, the increment is not substantial enough to offset the higher initial cost of larger batteries. For those reasons, the battery selected for the comparative analyses between direct and indirect configurations has a capacity of 75 Ah and 12 V, equating to 900 Wh.

Table 2. Maximum capacity of the battery, CAPEX of the configuration, utilization rate of PV energy, and net benefit of the configuration.

Capacity [Wh]	CAPEX [€]	PV rate [%]	Net benefit [€]
450	330,82	27,23	456,95
900	383,47	42,43	506,79
1350	414,52	43,32	493,93
1800	456,37	43,84	456,00

3. Results

3.1. Comparative H_2 Production

In the direct configuration, the PV generator and electrolyzer operate at the same current and voltage ($V_{\mathrm{PV}} = V_{\mathrm{EL}}$, $I_{\mathrm{PV}} = I_{\mathrm{EL}}$), determined by their intersecting current–voltage characteristics. Due to variations in G_t and T, the V_{PV} and I_{PV} typically do not match V_{MPP} and I_{MPP}. As a result, the PV generator provides suboptimal power ($P_{\mathrm{PV}} < P_{\mathrm{MPP}}$) to the electrolyzer (see Figure 2). This results in reduced H_2 production compared to the indirect configuration (regardless of the use of a battery), where H_2 production is directly proportional to I_{EL}, which equals I_{PV} but which is typically lower than I_{MPP} for most hours of the year in the direct configuration. To mitigate the disadvantages of direct coupling, we have designed the 200 W_p PV module (number and size of the PV cells) to optimize the H_2 production throughout the year (See Table 1). All three configurations under study in this work use the same 200 W_p module to ensure a fair comparison.

The indirect configurations include a PS with two steps: the MPPT and the DC–DC converter. The MPPT locks V_{MPP} and I_{MPP} in real time, extracting P_{MPP} from the PV generator in spite of the fluctuating G_t and T conditions. The DC–DC converter adjusts this $V_{\mathrm{MPP}} I_{\mathrm{MPP}}$ product to match the electrolyzer input power, defined by $V_{\mathrm{EL}} I_{\mathrm{EL}}$, with an efficiency η_{DC} so that:

$$\eta_{\mathrm{DC}} V_{\mathrm{MPP}} I_{\mathrm{MPP}} = V_{\mathrm{EL}} I_{\mathrm{EL}} \tag{6}$$

Ensuring the V_{EL}, I_{EL} pair fit the electrolyzer current-voltage characteristics. In this study, the DC–DC converter is assumed to have a constant efficiency of 95%.

Figure 3 shows the cumulative annual H_2 production (MH_2) for the three configurations studied. The direct configuration yields the least H_2, producing 4.61 kg per year. The indirect configuration without batteries produces a total of 5.41 kg of H_2 per year, which is 17.4% more than the direct configuration. As

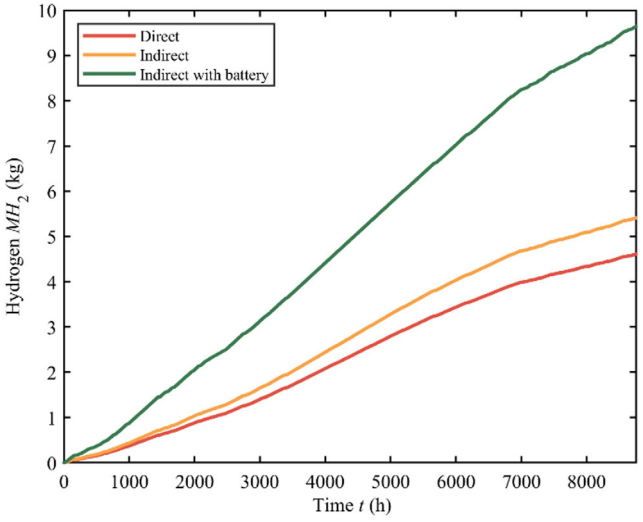

Figure 3. H_2 kilograms accumulated during the year (MH_2) for the direct and indirect (with and without battery) coupling configurations for aa a module PV Power of 200 W_p.

© 2024 The Author(s). Advanced Energy and Sustainability Research published by Wiley-VCH GmbH

observed in Figure 3, both the direct and indirect configurations without batteries exhibit the same trend, with increased production rates in spring and summer, due to higher G_t at the study location. It is observed that the MH_2 is similar during the first few months (approximately, the first 1400 h) of the year. After the first 1400 h, the difference in MH_2 is wider as the year progresses, with a clear advantage of the indirect configuration over the direct one. The indirect configuration with 900 Wh battery produces the most H_2 annually as shown in Figure 3, yielding 9.64 kg. This is 109% more than the direct configuration and 78.2% more than the indirect configuration without batteries. Similar to the other configurations, H_2 production is higher in the spring and summer months. However, in this case, the increase is much more pronounced (Figure 3), and H_2 production is significantly higher than in the configurations without batteries throughout the entire year.

The noticeable increase in the H_2 production rate during the spring and summer months is attributed to the numerous hours when the PV module generates more than 65 W. Consequently, the battery reaches its maximum charge nearly every day during these months. **Figure 4** illustrates the battery SOC throughout the year, showing higher SOC levels in the spring and summer compared to the beginning and end of the year. During the early and late months, the battery does not fully charge as often due to insufficient PV energy for H_2 production, leading to minor battery usage. However, in the central months, the battery charges fully each day, resulting in more continuous H_2 production compared to other periods.

3.2. Comparative Energy Production and Usage

The configurations can also be compared based on PV energy production and energy usage. For the sake of clarity, let us consider that the configurations produce usable energy if $I_{PV} - V_{PV}$ and $I_{EL} - V_{EL}$ intersect at a point in which $I \times V > 0$. We will also consider that the priority for the produced energy is to power the electrolyzer, and once it operates at its nominal power, the excess will be used to charge the battery (if there is any). In this way, only when the electrolyzer is operating at its nominal power and the battery is fully charged, will electricity be fed into the grid, which will be calculated as the subtraction of the energy used in electrolysis from the total energy produced. **Figure 5** shows the energy produced by each configuration (total bar height), the energy used for H_2 production (green fraction), and the surplus energy given to the grid (red fraction). The direct configuration produces 496 $kWh \cdot y^{-1}$, whereas the indirect configurations produce 565 $kWh \cdot y^{-1}$. The difference in total energy produced between the direct and indirect configurations (with and without battery) is due to situations in which for the same irradiance, G_t, and operation temperature, T, the direct configuration produces less electrical energy. The reason is that the intersection between the PV module current–voltage characteristic, $I_{PV} - V_{PV}$, and the electrolyzer current–voltage characteristic, $I_{EL} - V_{EL}$, is far from the optimum, that is, both curves do not intersect at the MPP. This leads to a lower total energy output of the direct configuration throughout the year, even including the energy losses associated with the efficiency of the PS in the indirect configurations. Regarding energy usage, Figure 5 shows that the direct configuration uses 208 $kWh \cdot y^{-1}$ for H_2 production, while 288 $kWh \cdot y^{-1}$ are considered surplus because they exceed the nominal 65 W of the electrolyzer. In other words, the direct configuration utilizes 41.9% of the energy for H_2 production, with 58.1% being fed into the grid. The indirect configuration without batteries uses 252 $kWh \cdot y^{-1}$ for H_2 production and has 313 $kWh \cdot y^{-1}$ as surplus, representing 44.6% and 55.4% of the produced energy, respectively. Compared to the direct configuration, the percentage of energy used for H_2 production by the indirect configuration is slightly higher but remains in the same range.

The indirect configuration with batteries uses 492 $kWh \cdot y^{-1}$ for H_2 production and has only 74 $kWh \cdot y^{-1}$ as surplus, representing 86.9% and 13.1% of the produced energy, respectively. Compared to the direct and indirect configurations without

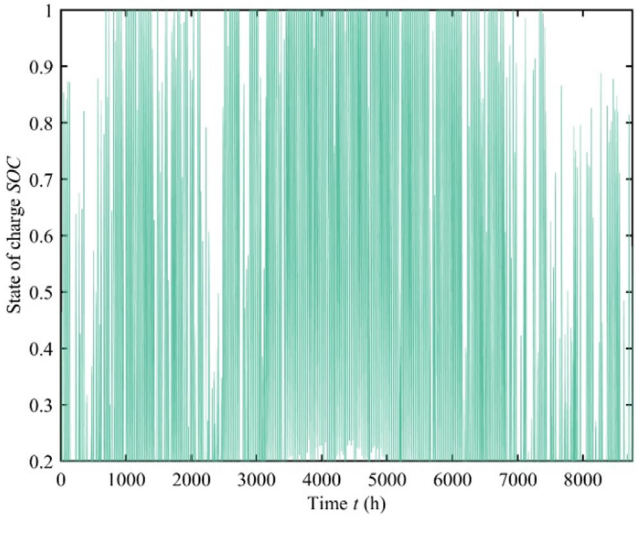

Figure 4. State of charge (SOC) of the 900 Wh battery used to store PV energy to maximize H_2 production during the year.

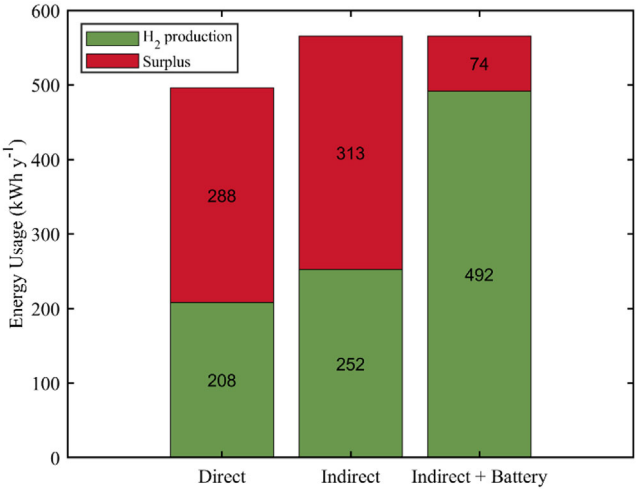

Figure 5. Energy production and usage in a year for the three configurations. All three configurations include a 200 W_p PV module and 65 W_p PEM electrolyzer while the indirect with battery also includes a 900 Wh C_{max} battery.

© 2024 The Author(s). Advanced Energy and Sustainability Research published by Wiley-VCH GmbH

batteries, the percentage of energy used for H_2 production is significantly higher. This explains why H_2 production is substantially greater in the battery configuration, as shown in Figure 3. The comparison of H_2 production and PV energy usage clearly indicates that the indirect configuration with 900 Wh battery storage is, by far, the most efficient in terms of energy. However, the economic perspective is crucial to determine whether the indirect configuration with batteries is viable.

3.3. Comparative Economic Viability

To conduct a brief economic feasibility study of the three configurations over the lifespan of the PEM electrolyzer (up to 80 000 h),[48–50] we will first calculate the costs for each configuration. The costs (C) include initial investment (CAPEX) and annual operational expenses (OPEX):

$$C = \text{CAPEX} + \text{OPEX} \tag{7}$$

The CAPEX includes the costs of the main components for each configuration, as well as the energy balance of the system (EBOS) and the structure balance of the system (SBOS). The EBOS refers to all the electrical and electronic components that are necessary for the operation of the green H_2 production system but are not part of the main production unit itself (e.g., electrical infrastructure, control systems, cabling, etc.). The SBOS refers to the physical and structural components required to support and house the system (e.g., physical structures, support systems, piping and plumbing, safety systems, site preparation, etc.). Together, EBOS and SBOS ensure that the green hydrogen production system operates efficiently, safely, and reliably, integrating all necessary auxiliary components and infrastructure. **Table 3** shows the cost of every individual main component (PV module, electrolyzer, PS, and battery), as well as the EBOS, SBOS, and OPEX of the entire system. The cost of SBOS and EBOS per unit of power is based on PV power. Table 3 also includes the cost per power unit ($€ \cdot W^{-1}$) of the PV module, electrolyzer, and PS, as well as the energy storage unit ($€ \cdot Wh^{-1}$) in the case of the battery. It should be noted that all these costs provide an underestimated figure, as they do not include expenses for the engineering project, land, labor, permits, taxes, and other related items for simplicity. Finally, the lifespan and total cost of the different components are also defined in the table. All configurations include OPEX, SBOS, and EBOS in their cost, but the components are not the same in every configuration. The direct configuration only includes the PV module and the electrolyzer. The indirect configuration without batteries also includes the PS, and finally, the indirect configuration with batteries includes all elements presented in Table 3

Table 3. Cost per power unit, energy unit, lifespan, and total cost of the components used in the different configurations.

Component	Cost	Lifespan [h]	Unit	Cost [€]
200 W_p PV module	0.345 $€ \cdot W^{-1}$ [66]	2.19×10^5	1	69.0
65 W_p Electrolyzer	1.071 $€ \cdot W^{-1}$ [67]	8.70×10^4	1	69.6
PS	0.045 $€ \cdot W^{-1}$ [66]	1.31×10^5	1	16.1
Battery	0.120 $€ \cdot Wh^{-1}$ [68]	1.31×10^5	1	105.5
Regulator	0.140 $€ \cdot W^{-1}$ [69]	1.31×10^5	1	27.9
EBOS	0.160 $€ \cdot W^{-1}$ [66]	–	1	32.6
SBOS	0.120 $€ \cdot W^{-1}$ [66]	–	1	23.8
OPEX	0.025 $€ \cdot W^{-1}y^{-1}$ [66]	–	1	5.0

The gross benefits (B_g) are also accounted in this study, which depend on the annual amount of H_2 produced (MH_2) and the surplus PV energy fed into the grid (E_x).

$$B_g = n \cdot [(MH_2 \cdot PH_2) + (E_x \cdot PE_x)] \tag{8}$$

To simplify the economic feasibility study, we assume that the prices of H_2 (PH_2) and surplus energy (PE_x) remain stable over the years, which are 10 $€ \cdot kg^{-1}$ and 0.05 $€ \cdot kWh^{-1}$, respectively.[51,52] To determine the economic viability of each configuration over the 9-year lifespan of the PEM electrolyzer, we calculate the net benefits (B_n), which are derived by subtracting C to B_g. The configuration with the highest B_n at the end of year 9 will be the most economically profitable. In the small-scale examples of the three configurations we have used in our study, the initial cost of the direct configuration is €200, the indirect configuration without batteries is €216, and the indirect configuration with a 900 Wh battery is €349. According to these initial costs, **Figure 6** shows the evolution of the net benefits of the three configurations over the 9-year lifespan of the PEM electrolyzer. A configuration becomes profitable when net benefits transition from negative to positive, crossing the zero-line indicated in Figure 6.

Figure 6 also shows that all configurations become profitable by the end of the study. All three configurations become profitable after year 3. Despite the higher initial cost of the indirect configuration without a battery compared to the direct one, the former produces more annual H_2 (Figure 3 and 5) and feeds more surplus electricity to the grid (Figure 5). This results in a faster rate of profit generation for the indirect configuration. In

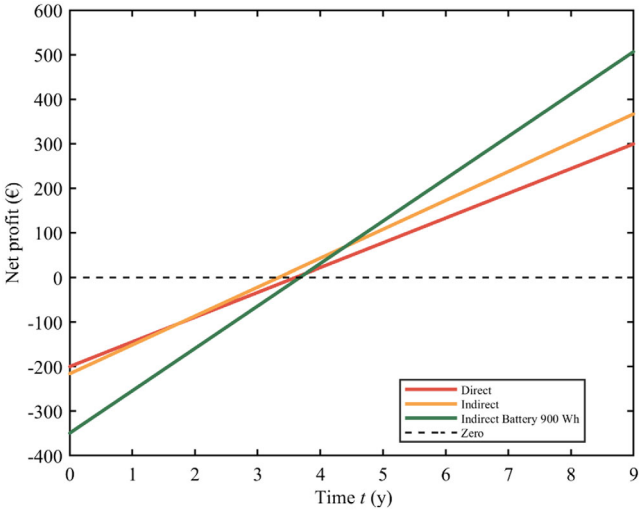

Figure 6. Net profit evolution of the three configurations throughout the 9-year lifespan of the electrolyzer.

© 2024 The Author(s). Advanced Energy and Sustainability Research published by Wiley-VCH GmbH

fact, by year 9, the indirect configuration without battery is more profitable than the direct configuration, generating €366.9 and €299.6, respectively. The indirect configuration with 900 Wh battery is the most expensive from the start (Figure 6), primarily due to the cost of the battery, the most expensive component. However, it is also the most profitable configuration by the end of year 9, generating €506.8 in net benefits. In terms of € per PV W_p, the net profit of direct configuration is 1.49 $€ \cdot W^{-1}$, the indirect configuration without battery is 1.83 $€ \cdot W^{-1}$ while net benefit of the indirect configuration with 900 Wh is 2.53 $€ \cdot W^{-1}$ after 9 years.

If the electrolyzer lifetime is less than 80 000 h, the gap in net profitability between the different configurations narrows (Figure 6). In fact, the findings of this article are valid if the PEM electrolyzers have a lifespan of more than 4 years, as this is the time frame within which all configurations become profitable, according to the results from Figure 6.

Thus, after comparing H_2 production, PV energy generation, energy usage, and economic profitability across the three configurations, considering the costs of the various components chosen in this study for the S-H system and the prices of the byproducts obtained from it, the indirect configuration with batteries is the smartest option for optimizing the entire H_2 production process using solar PV energy.

4. Conclusions

A comparative analysis has been conducted between the direct and indirect (with and without battery) configurations for annual H_2 production, energy usage, and economic viability. The results show clear advantage of the indirect configuration with a 900 Wh battery because: 1) produces 9.64 kg of H_2 annually, compared to the 4.61 and 5.41 kg of the direct and indirect configuration without battery; 2) uses 86.9% of the PV energy to produce H_2 compared to 41.9% and 44.6% of the direct and indirect configurations; and 3) is the most profitable one in the lifespan of the PEM electrolyzer, generating 2.53 $€ \cdot W^{-1}$ compared to 1.49 $€ \cdot W^{-1}$ and 1.83 $€ \cdot W^{-1}$ of the direct and indirect configurations.

Appendix

Thermodynamically, under the assumption of reversible processes, $\Delta G_{R,0}$ represents the minimum electrical work required to drive the electrolysis reaction at constant pressure and temperature. This implies that each electron flowing through the circuit possesses an energy qV_{rev}, defined by:

$$qV_{rev} = q\frac{\Delta G_{R,0}}{ZF} = 1.23\,\text{eV} \tag{A1}$$

with Z representing the moles of electrons produced per mole of water in the reaction ($Z = 2$), and F being the Faraday constant (96 500 C mol^{-1}) the energy per electron corresponds to the minimum voltage necessary ($V_{rev} = 1.23\,V$) for an electric current to flow through the electrolyzer, thus enabling electrolysis. In practical scenarios, additional electrical work is required due to the lack of an external heat source to maintain a constant temperature and the presence of irreversible processes. Consequently, the threshold voltage ($V_{th,c}$) needed for the reaction to occur exceeds V_{rev}. Various empirical expressions to determine $V_{th,c}$ are available in the literature, for instance:[53]

$$V_{th,c} = -(1-k)\frac{\Delta G_{R,0}}{ZF} \tag{A2}$$

where k counts for the presence of these nonidealities. In our experience working with electrolyzers, $k = 2.12$ seems a reasonable choice which leads to $V_{th,c} = 1.38\,V$

The activation overpotential is associated with the activation energy needed by the electrodes to facilitate their respective reactions. It has two contributions, $V_{act,a}$ and $V_{act,c}$ for the anode and cathode respectively so that:

$$V_{act} = V_{act,a} + \left|V_{act,c}\right| \tag{A3}$$

The Butler–Volmer equation is often used for calculating these overpotentials:[43,54]

$$V_{act,a} = \frac{RT}{\alpha_a ZF}\text{arcsinh}\left(\frac{I_{EL}}{2A_{EL}j_{0,a}}\right) \tag{A4}$$

$$V_{act,c} = -\frac{RT}{\alpha_c ZF}\text{arcsinh}\left(\frac{I_{EL}}{2A_{EL}j_{0,c}}\right) \tag{A5}$$

In these equations, R is the gas constant (8.314 $JK^{-1}mol^{-1}$), α_a and α_c are the charge transfer coefficients for the anode and cathode, respectively, $j_{0,a}$ and $j_{0,c}$ are the exchange current densities for anode and cathode and A_{EL} is the effective area of the electrolyzer for current transport. For simplicity this study assumes $\alpha_a = \alpha_c = 0.5$.[43] Other authors have proposed simplified equations,[55,56] which are valid when I_{EL} is larger than $A_{EL}j_{0,ref}$, making it suitable for our case:

$$V_{act,a} = \frac{RT}{\alpha_a ZF}\ln\left(\frac{I_{EL}}{A_{EL}j_{0,a}}\right) \tag{A6}$$

Table A1.

Electrolyzer parameter		References
Maximum current density, j_L [A cm^{-2}]	4.00	[57]
Anode exchange current density, $j_{0,a\,ref}$ [A cm^{-2}]	1.00×10^{-7}	[57]
Cathode exchange current density, $j_{0,c\,ref}$ [A cm^{-2}]	1.00×10^{-3}	[57]
Charge transfer coefficients, α_a, α_c	0.500	[58]
Activation energy, E_{exc} [J mol^{-1}]	5.40×10^4	[24]
PEM conductivity at T_{ref}, σ_{ref} [S cm^{-1}]	2.00×10^{-2}	[59]
PEM Activation energy for H^+ transport, E_{pro} [J mol^{-1}]	1.89×10^4	[24]
PEM thickness, t_m [cm]	1.83×10^{-2}	[59]
Electrolyzer cell effective area, A_{EL} [cm^2]	8.75	–
Reference temperature, T_{ref} [K]	353	[57]
Number of electrolytic cells, S_{cell}	6.00	–
Threshold voltage nonideality factor, k	2.12	–

© 2024 The Author(s). Advanced Energy and Sustainability Research published by Wiley-VCH GmbH

$$V_{act,c} = -\frac{RT}{\alpha_c ZF}\ln\left(\frac{I_{EL}}{A_{EL} j_{0,c}}\right) \tag{A7}$$

Regarding $j_{0,a}$ and $j_{0,c}$, the values reported in the literature vary significantly. Consequently, some authors choose values that best fit their specific models.[46,49] Given the temperature dependence of these parameters, an expression that relates them to temperature is particularly useful. Such a relationship is often described in the literature using an Arrhenius-type equation, expressed as follows:

$$j_0 = j_{0,ref} \exp\left[-\frac{E_{exc}}{R}\left(\frac{1}{T} - \frac{1}{T_{ref}}\right)\right] \tag{A8}$$

where $j_{0,ref}$ is a reference value obtained from literature or experimentally,[57] T_{ref} is the temperature at which $j_{0,ref}$ is measured, and E_{exc} is the activation energy of the reaction.

Similar to V_{act}, the concentration overpotential V_{con} has both anodic and cathodic contributions. However, the anodic contribution is significantly higher and will thus be the sole focus of this study. It can be modeled using the following expression:[56]

$$V_{con} = \frac{RT}{\alpha_a ZF}\ln\left(\frac{j_L}{j_L - I_{EL}/A_{EL}}\right) \tag{A9}$$

where j_L is the limiting current density, which is the maximum current density that can be provided to the electrolyzer. This overpotential is paramount for high current densities ($\approx$4 A cm^{-2}) and substantially lowers the efficiency when present.[57]

Regarding the overpotential due to ohmic losses, this can be modeled as:

$$V_{ohm} = \frac{I_{EL} r_{ohm}}{A_{EL}} \tag{A10}$$

where r_{ohm} is the electric resistance by unit of area of the PEM membrane to H^+ ions transport. This resistance by unit of area depends on the membrane thickness (t_m) and electric conductivity (σ) as follows:

$$r_{ohm} = \frac{t_m}{\sigma} \tag{A11}$$

The conductivity can be modeled with an Arrhenius type expression:

$$\sigma = \sigma_{ref} \exp\left[-\frac{E_{pro}}{R}\left(\frac{1}{T} - \frac{1}{T_{ref}}\right)\right] \tag{A12}$$

where E_{pro} is the activation energy for proton transport in the membrane and σ_{ref} is the conductivity of the membrane at T_{ref}.

Parameters of the electrolyzer are presented in the table below.

Acknowledgements

This work is sponsored by the Project CEOTRES-CM (Y2020/EMT-6419) funded by the Comunidad de Madrid.

Conflict of Interest

The authors declare no conflict of interest.

Author Contributions

Alfonso González del Valle: Conceptualization (supporting); Data curation (equal); Formal analysis (equal); Investigation (equal); Methodology (supporting); Software (lead); Visualization (lead); Writing—original draft (lead); Writing—review & editing (equal). **Pablo García-Linares**: Conceptualization (equal); Formal analysis (equal); Investigation (equal); Methodology (lead); Supervision (equal); Validation (equal); Writing—review & editing (equal). **Antonio Martí**: Formal analysis (equal); Funding acquisition (lead); Investigation (equal); Methodology (equal); Project administration (lead); Resources (lead); Supervision (equal); Validation (equal); Writing—review & editing (equal).

Data Availability Statement

The data that support the findings of this study are available from the corresponding author upon reasonable request.

Keywords

battery storage, direct and indirect configurations, economic viability, hydrogen production, photovoltaics

Received: July 15, 2024
Revised: October 14, 2024
Published online:

[1] A. Kovač, M. Paranos, D. Marciuš, *Int. J. Hydrogen Energy* **2021**, *46*, 10016.
[2] F. Swennenhuis, V. de Gooyert, H. de Coninck, *Energy Res. Soc. Sci.* **2022**, *88*, 102598.
[3] D. R. Nhuchhen, S. P. Sit, D. B. Layzell, *Appl. Energy* **2022**, *317*, 119180.
[4] N. Rambhujun, M. S. Salman, T. Wang, C. Pratthana, P. Sapkota, M. Costalin, Q. Lai, K.-F. Aguey-Zinsou, *MRS Energy Sustainability* **2020**, *7*, 33.
[5] S. Atilhan, S. Park, M. M. El-Halwagi, M. Atilhan, M. Moore, R. B. Nielsen, *Curr. Opin. Chem. Eng.* **2021**, *31*, 100668.
[6] F. Schenke, J. Hoelzen, C. Minke, A. Bensmann, R. Hanke-Rauschenbach, *Energy Convers. Manage.: X* **2023**, *20*, 100435.
[7] G. Russell, A. Nenov, J. T. Hancock, *Appl. Sci.* **2024**, *14*, 2877.
[8] O. Tang, J. Rehme, P. Cerin, *Energy* **2022**, *241*, 122906.
[9] A. Peppas, S. Kottaridis, C. Politi, *Mater. Proc.* **2023**, *15*, 30.
[10] J. A. Faria, *Curr. Opin. Green Sustainable Chem.* **2021**, *29*, 100466.
[11] A. Mraoui, B. Benyoucef, L. Hassaine, *Int. J. Hydrogen Energy* **2018**, *43*, 3441.
[12] G. M. Sriramagiri, W. Luc, F. Jiao, K. Ayers, K. D. Dobson, S. S. Hegedus, *Sustainable Energy Fuels* **2019**, *3*, 422.
[13] L. Phan Van, L. Hieu Hoang, T. Nguyen Duc, *Int. J. Hydrogen Energy* **2023**, *48*, 25231.
[14] M. Biswal, S. Sabyasachi, *Int. J. Eng. Res. Appl.* **2012**, *2*.
[15] X. Gu, Z. Ying, X. Zheng, B. Dou, G. Cui, *Renewable Energy* **2023**, *209*, 53.
[16] X. Hu, L. Xu, X. Lin, M. Pecht, *Joule* **2020**, *4*, 310.
[17] V. K. Bupesh Raja, I. Raja, R. Kavvampally, *J. Phys.: Conf. Ser.* **2021**, *2129*, 012011.

© 2024 The Author(s). Advanced Energy and Sustainability Research published by Wiley-VCH GmbH

[18] M. Scarfogliero, S. Carmeli, F. Castelli-Dezza, M. Mauri, M. Rossi, G. Marchegiani, E. Rovelli, in *2018 Int. Conf. Electrical and Electronic Technologies for Automotive*, IEEE, Milan **2018**, pp. 1–6.
[19] M. J. Lacey, A. Yalamanchili, J. Maibach, C. Tengstedt, K. Edström, D. Brandell, *RSC Adv.* **2016**, *6*, 3632.
[20] L. Arriaga, W. Martinez, U. Cano, H. Blud, *Int. J. Hydrogen Energy* **2007**, *32*, 2247.
[21] B. Paul, *Int. J. Hydrogen Energy* **2008**, *33*, 490.
[22] F. Gutiérrez-Martín, L. Amodio, M. Pagano, *Int. J. Hydrogen Energy* **2021**, *46*, 29038.
[23] F. Gutiérrez-Martín, J. A. Díaz-López, A. Caravaca, A. J. Dos Santos-García, *Int. J. Hydrogen Energy* **2024**, *52*, 995.
[24] R. García-Valverde, N. Espinosa, A. Urbina, *Int. J. Hydrogen Energy* **2011**, *36*, 10574.
[25] R. E. Clarke, S. Giddey, F. T. Ciacchi, S. P. S. Badwal, B. Paul, J. Andrews, *Int. J. Hydrogen Energy* **2009**, *34*, 2531.
[26] A. González Del Valle, P. García-Linares, A. Martí, *Energy Convers. Manage.* **2024**, *315*, 118751.
[27] O. Astakhov, S. N. Agbo, K. Welter, V. Smirnov, U. Rau, T. Merdzhanova, *J. Power Sources* **2021**, *509*, 230367.
[28] O. Astakhov, T. Merdzhanova, L.-C. Kin, U. Rau, *Sol. Energy* **2020**, *206*, 732.
[29] G. Soyturk, O. Kizilkan, M. A. Ezan, C. O. Colpan, *Int. J. Hydrogen Energy* **2024**, *67*, 1181.
[30] S. Avril, G. Arnaud, A. Florentin, M. Vinard, *Energy* **2010**, *35*, 5300.
[31] M. W. Chamout, A. Perl, E. J. Hengeveld, J. Aué, *Int. J. Hydrogen Energy* **2024**, *70*, 170.
[32] R. Muthia, A. S. P. Pramudya, M. R. Maulana, W. W. Purwanto, *Clean Energy* **2024**, *8*, 1.
[33] Y. Kikuchi, T. Ichikawa, M. Sugiyama, M. Koyama, *Int. J. Hydrogen Energy* **2019**, *44*, 1451.
[34] N. Sako, M. Koyama, T. Okubo, Y. Kikuchi, *J. Cleaner Prod.* **2021**, *298*, 126809.
[35] PVGIS-SARAH2, European Commission, https://re.jrc.ec.europa.eu/pvg_tools/en/ (accessed: March 2023).
[36] F. Ghani, G. Rosengarten, M. Duke, J. K. Carson, *Renewable Energy* **2014**, *72*, 105.
[37] G. Ciulla, V. Lo Brano, V. Di Dio, G. Cipriani, *Renewable Sustainable Energy Rev.* **2014**, *32*, 684.
[38] H. K. Mehta, H. Warke, K. Kukadiya, A. K. Panchal, *IEEE J. Photovoltaics* **2019**, *9*, 803.
[39] J. Ramos-Hernanz, J. M. Lopez-Guede, E. Zulueta, *WSEAS Trans. Power Syst.* **2017**, *12*, 231.
[40] S. A. Rahman, R. K. Varma, T. Vanderheide, *IET Renewable Power Gener.* **2014**, *8*, 217.
[41] A. Rabiee, A. Keane, A. Soroudi, *Renewable Energy* **2021**, *163*, 1580.
[42] S. Shiva Kumar, H. Lim, *Energy Rep.* **2022**, *8*, 13793.
[43] D. S. Falcão, A. M. F. R. Pinto, *J. Cleaner Prod.* **2020**, *261*, 121184.
[44] P. Millet, in *Electrochemical Power Sources: Fundamentals, Systems, and Applications* (Eds: T. Smolinka, J. Garche), Elsevier, Amsterdam, Netherlands **2022**, pp. 37–62, Ch. 2.
[45] K. Raj Kapur, S. Paulson, *Int. J. Hydrogen Energy* **2024**, *82*, 1.
[46] L. Rui, L. Ying, X. Ji, H. Jiawei, *Appl. Energy* **2022**, *326*, 120011.
[47] H. P. C. Buitendach, R. Gouws, C. A. Martinson, C. Minnaar, D. Bessarabov, *Results Eng.* **2021**, *10*, 100216.
[48] E. Kuhnert, V. Hacker, M. Bodner, *Int. J. Energy Res.* **2023**, *2023*, 1.
[49] E. Van Der Roest, R. Bol, T. Fens, A. Van Wijk, *Int. J. Hydrogen Energy* **2023**, *48*, 27872.
[50] O. Schmidt, A. Gambhir, I. Staffell, A. Hawkes, J. Nelson, S. Few, *Int. J. Hydrogen Energy* **2017**, *42*, 30470.
[51] K. Schelling, *Green Hydrogen to Undercut Gray Sibling by End of Decade, BloombergNEF* **2023**, https://about.bnef.com/blog/green-hydrogen-to-undercut-gray-sibling-by-end-of-decade/.
[52] Precio de los excedentes de autoconsumo en PVPC para hoy, Selectra, https://selectra.es/autoconsumo/info/tarifas/pvpc (accessed: June 2024).
[53] H. Kim, M. Park, K. S. Lee, *Int. J. Hydrogen Energy* **2013**, *38*, 2596.
[54] Z. Abdin, C. J. Webb, E. M. A. Gray, *Int. J. Hydrogen Energy* **2015**, *40*, 13243.
[55] A. E.-S. A. Nafeh, *Int. J. Numer. Modell. Electron. Networks Devices Fields* **2011**, *24*, 282.
[56] R. García-Valverde, N. Espinosa, A. Urbina, *Int. J. Hydrogen Energy* **2012**, *37*, 1927.
[57] P. Choi, *Solid State Ionics* **2004**, *175*, 535.
[58] S. Touré, A. Konaté, D. Traoré, D. Fofana, *IOP Conf. Ser.: Earth Environ. Sci.* **2018**, *188*, 012041.
[59] Nafion Sulfonic Membranes, Nafion, https://www.nafion.com/en/products/sulfonic-membranes (accessed: March 2024).
[60] J. Müller, K. Bothe, S. Herlufsen, H. Hannebauer, R. Ferré, R. Brendel, *Sol. Energy Mater. Sol. Cells* **2012**, *106*, 76.
[61] M. A. Green, E. D. Dunlop, G. Siefer, M. Yoshita, N. Kopidakis, K. Bothe, X. Hao, *Prog. Photovoltaics* **2023**, *31*, 3.
[62] P. Singh, N. M. Ravindra, *Emerging Mater. Res.* **2012**, *1*, 33.
[63] H. Lin, G. Wang, Q. Su, C. Han, C. Xue, S. Yin, L. Fang, X. Xu, P. Gao, *Prog. Photovoltaics* **2024**, *32*, 359.
[64] O. Dupre, R. Vaillon, M. A. Green, *IEEE J. Photovoltaics* **2016**, *6*, 56.
[65] Q. Wang, B. Xu, J. Sun, H. Liu, Z. Zhao, D. Yu, C. Fan, J. He, *J. Am. Chem. Soc.* **2014**, *136*, 9826.
[66] V. Ramasamy, J. Zuboy, M. Woodhouse, E. O'Shaughnessy, D. Feldman, J. Desai, A. Walker, R. Margolis, P. Basore, *Renewable Energy* **2023**.
[67] S. Krishnan, V. Koning, M. Theodorus De Groot, A. De Groot, P. G. Mendoza, M. Junginger, G. J. Kramer, *Int. J. Hydrogen Energy* **2023**, *48*, 32313.
[68] Lithium-Ion Battery Pack Prices Hit Record Low of $139/kWh, BloombergNEF, https://about.bnef.com/blog/lithium-ion-battery-pack-prices-hit-record-low-of-139-kwh/ (accessed: July 2024).
[69] K. S. Awale, A. U. Kumbhar, V. A. Kole, J. B. Kamate, *J. Electr. Electron. Syst.* **2017**, *6*, 1000221.

© 2024 The Author(s). Advanced Energy and Sustainability Research published by Wiley-VCH GmbH